Science Advances
AAAS

advances.sciencemag.org/cgi/content/full/6/29/eabb0425/DC1

Supplementary Materials for

Aerosol-forced multidecadal variations across all ocean basins in models and observations since 1920

Minhua Qin, Aiguo Dai*, Wenjian Hua*

*Corresponding author. Email: adai@albany.edu (A.D.); whua.atmos@gmail.com (W.H.)

Published 17 July 2020, *Sci. Adv.* **6**, eabb0425 (2020)
DOI: 10.1126/sciadv.abb0425

This PDF file includes:

Supplementary Text
Figs. S1 to S8
Tables S1 and S2
References

Supplementary Text

S1. The detrending approach

Prior methods used to define the forced signal and internal variability (IV) in observations and assess their relative roles include: (1) using simple linear detrending to remove the forced long-term trend (which leaves forced decadal variations in the residual) *(18)*, which is not a good choice since the long-term warming signal is non-linear in time and non-uniform in space (*14, 19*); (2) using the observed global-mean SST time series to represent the externally-forced change (*19*), which is incorrect since the global-mean temperature from individual ensembles contains internal variations and differ from each other (*45*); and (3) using the ensemble mean of climate model ensemble simulations to estimate the externally-forced change and consider the residual in any realization (such as a model run or the observations) as the internal variations after the forced component being removed through regression (the method used in our study). We have tested these different methods to separate the externally-forced and internally-generated variations in the North Atlantic and Pacific (i.e., to define the AMO and IPO index, *11*, *17*; not shown), and method 3 outperforms the other methods. As the global-mean SST time series from the ensemble mean mainly contains a forced response, this procedure removes most of the externally-forced component from the observations (*44*).

To remove the warming effect from the monotonic increase in greenhouse gases (GHGs), we detrended the observational SSTs using global-mean SST time series from the ensemble mean of the CMIP5 GHG-only simulations.

S2. The statistical significance

The statistical significance of the correlations and regressions between two time series, especially after applying low-pass filter, is an important issue. To account for the reduced degree of freedom caused by the low-pass filtering, we used the effective degrees of freedom (EDF) to account for autocorrelation in estimating the attained significance (i.e., the p-value) in the Student's t-test. The EDF (N*) is given by the following approximation (*8, 46*):

$$\frac{1}{N*} \approx \frac{1}{N} + \frac{2}{N}\sum_{j=1}^{N}\frac{N-j}{N}\rho\mathrm{xx(j)}\rho\mathrm{yy(j)} \ ,$$

where N is the sample size, and ρxx(j) and ρyy(j) are the autocorrelations of the two sampled time-series x and y at time lag j. Our method, which is based on Zhao and Khalil (*47*), is similar to the above equation but without the weighting function (N-j)/N. This method performed relatively well compared to other methods (*46*). We also repeated the analysis directly using the above equation in estimating EDF, and the results are similar.

Furthermore, we also used the Monte Carlo approach to derive the attained significance. The Monte Carlo approach was implemented as follows: For each of the x and y variables, its time series was first randomized in its temporal order to generate 1,000 synthetic time series for each of them, the correlation coefficient for each pair of these 1,000 samples was then computed, and a probability density function of the correlation coefficients was estimated to assess the statistical significance of the attained correlation coefficient between x and y. The quoted significance level (i.e., the p-value) is the fraction of the samples whose r values exceed the value being tested. The p-values from this Monte Carlo approach are similar to those from the Student's t-test with EDF shown in Fig. 1C and Fig. 2, except for the negative correlations in the tropical central Pacific and subtropical South Atlantic, where the Monte Carlo approach

suggests a lower significance level. Note that the negative correlations in the tropical central Pacific and subtropical South Atlantic are dominated by the IV component (e.g., IPO-like variability, *7*, *17*, *44*), where SSTs have weaker autocorrelation than other regions (e.g., ATL, TWP, SNP, SSP) that are dominated by the externally-forced component.

S3. Estimated GHG-detrend forced component

Separating different externally-forced components in the observations or model simulations is not a trivial task. We have tested three ways to estimate the GHG-detrend forced component (i.e., externally-forced decadal-multidecadal signal) including:

1) The GHG-detrend forced component is estimated by using the low-passed filtered SST anomalies from the CMIP5 all-forcing MMM after removing the GHG-induced warming signal via linear regression. We removed the GHG-induced warming via linear regression from the CMIP5 all-forcing MMM and then averaged the residual SSTs to derive the GHG-detrend forced decadal signal.

2) The forced decadal signal was estimated based on the regressed SSTs between local smoothed SSTs from observations and the global-mean SST time series from the GHG-detrended SST fields from the CMIP5 all-forcing MMM. This method accounts for the potential biases in model simulated response, but may alias correlated but unforced SST changes into this estimate (not shown).

3) We removed the GHG-forced changes, which is represented by the global-mean SST time series derived from the CMIP5 GHG-only MMM from the observed SSTs via linear regression, to obtain the GHG-detrend component in the observations. We also removed the changes and variations at each grid point associated with the forced signal, which is represented by the global-mean SST time series from the CMIP5 all-forcing historical MMM from the observed SST time series via linear regression, to derive the estimated internal variability. The difference between the two represents the estimated externally-forced decadal-multidecadal variations in observed SSTs (see Fig. 2 for details).

Overall, three methods produce similar decadal-multidecadal forced signal, indicating that the results are not sensitive to the choice of estimation methods, although the magnitudes and variations of forced signal may slightly differ over the six regions among these approaches.

S4. Greenhouse forcing effect on Indian Ocean

For the Indian Ocean, the observed SST changes are largely accounted for by the GHG forcing alone, with only small multidecadal variations unexplained (not shown), which is consistent with Dong et al. (*48*), who found that anthropogenic forcing has dominated the Indian Ocean basin-wide warming trend since the 1950s. The large anomalies during the early 1940s are likely due to sufficient observations and changes in data sources (*38-41*) during the 2nd World War. This occurred in all other regions (Fig. 2).

S5. Aerosols' indirect effect on climate variability

Aerosol indirect effects (AIE) through their impacts on cloud microphysics and lifetime account for about 50-60% of the total global aerosols' impact, with larger impacts over oceans (*10, 17*). However, most of the climate models neglect the AIE, which could potentially lead to an underestimate of aerosols' effect when using the multi-model ensemble mean.

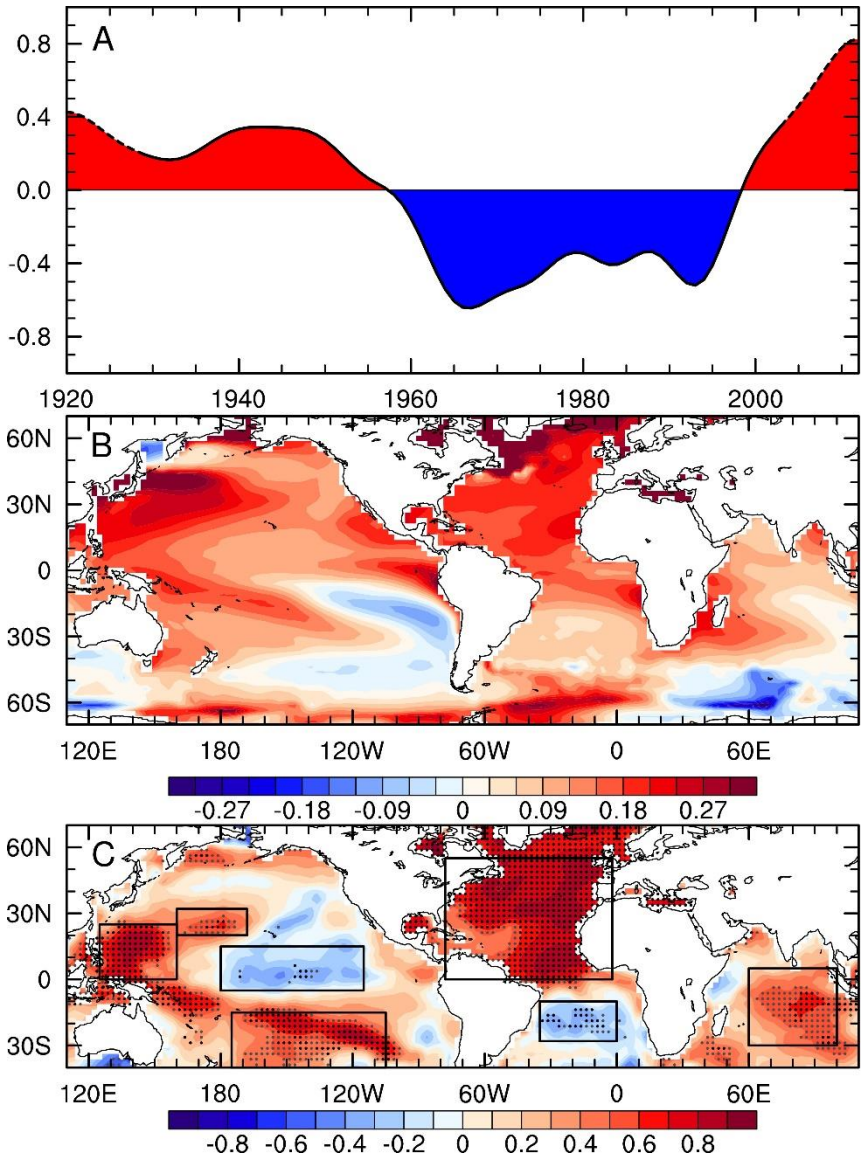

Fig. S1. Multidecadal SST variations in models and observations. (**A**) Time series of the principal component (PC) and (**B**) spatial pattern of the leading EOF mode in the global low-pass filtered SST fields from the CESM1 large ensemble mean of all-forcing historical simulations from 1920-2012 after the GHG-induced warming signal was removed. We detrended the CESM1 ensemble mean at each grid point using the global-mean SST time series derived from the CMIP5 multi-model ensemble mean (MMM) of the GHG-forcing-only simulations via linear regression. (**C**) Correlation map between the PC time series in (A) and the local low-pass filtered SST anomalies from observations from 1920-2012. We removed the GHG-induced warming signal from the observations through linear regression using the global-mean SST time series derived from the CMIP5 MMM of the GHG-forcing-only simulations. The black (gray) stippling indicates that the correlation is statistically significant at the 0.05 (0.1) level based on a two-sided Student's t-test with an estimated effective degree of freedom to account for autocorrelation. We used a 19-point Lanczos filter with a 13-year cutoff period to smooth the data. Results are similar using 13-year moving averaged data. The ensemble size is 35 for the CMIP5 GHG-forcing- only simulations.

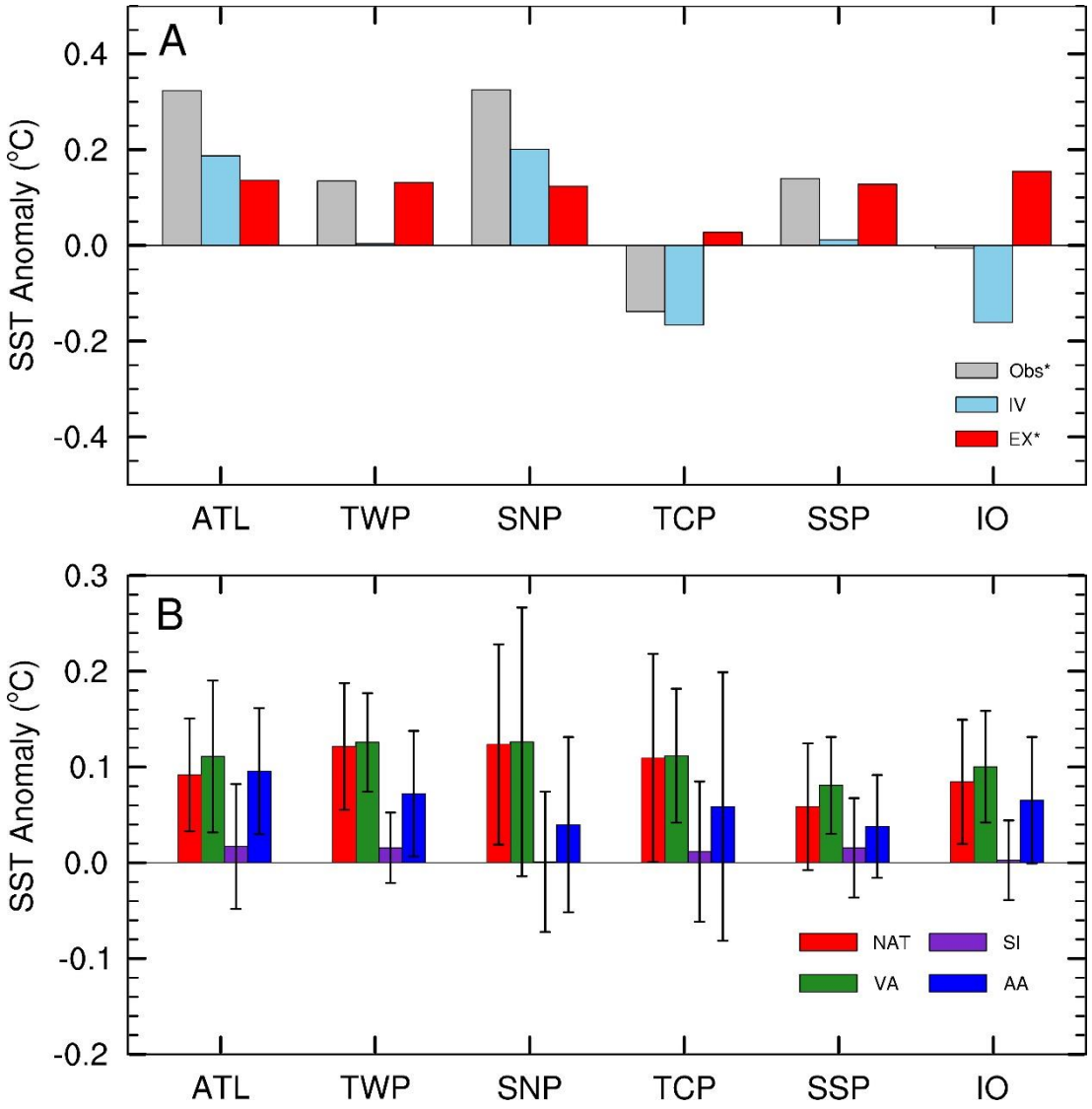

Fig. S2. Contributions of internal variability and external forcing. (**A**) Annual-mean SST anomalies (°C) for the two warm periods (1950-1960 and 1998-2012) relative to the intervening cold period (1970-1995) from observations (Obs*, gray), internal variability (IV, blue, as in Fig. 2), and external forcing (EX*, red) with the GHG-induced change being removed in the Obs* and EX* cases as in Fig. 2. The warm and cold periods were selected based on the EX* variations shown in Fig. 2. (**B**) Annual-mean SST anomalies (°C) during the warm periods (1950-1960 and 1998-2005) relative to the cold period (1970-1995) estimated from the CMIP5 natural (NAT), volcanic aerosol (VA), solar irradiance (SI) and anthropogenic aerosol (AA) single forcing simulations. The single forcing simulations were linearly detrended before calculating the anomalies in order to highlight the decadal variations. The error bars denote the ±1 standard deviation of the inter-model variations.

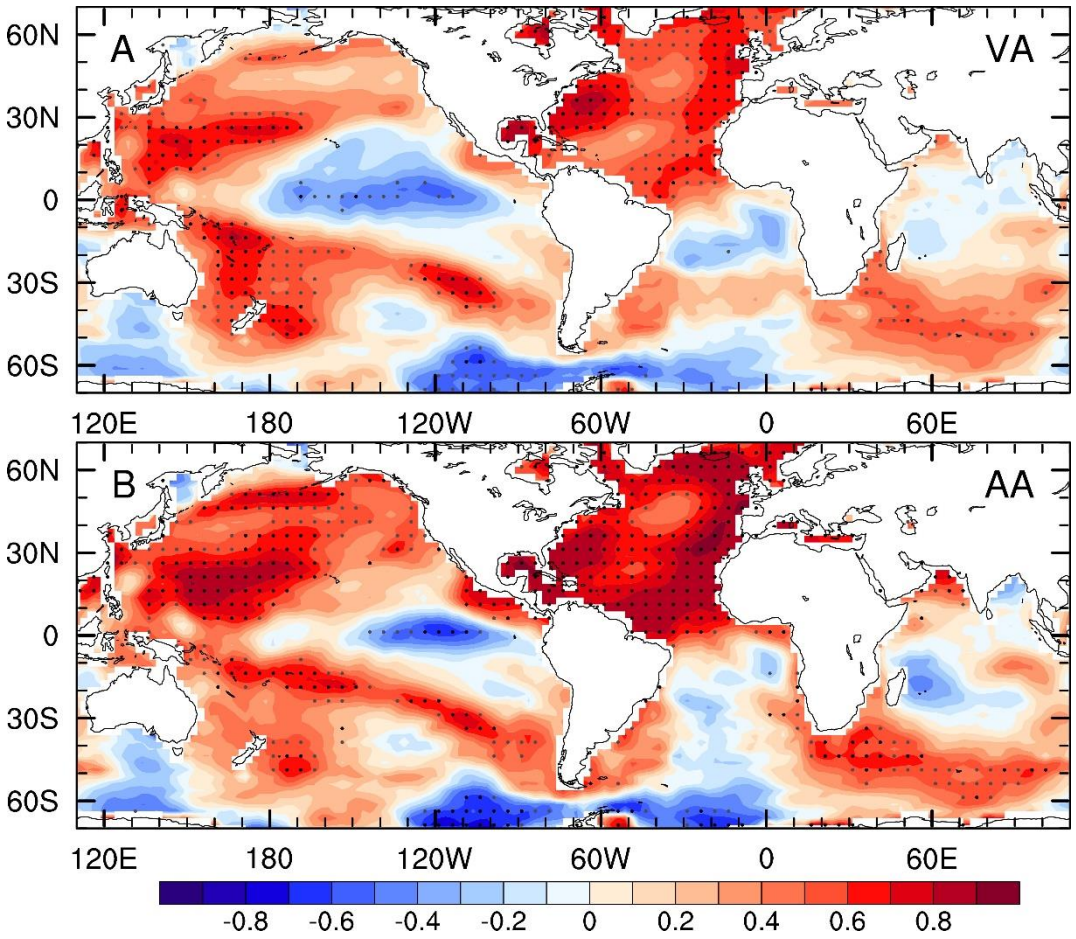

Fig. S3. Relationship between SST and aerosol forcing. Correlation maps between the low-pass filtered local SST anomalies from observations (with the GHG-induced warming removed) and the PC time series of the leading EOF in the near-global linearly detrended, low-pass filtered SST fields from the MMM of CMIP5 (**A**) VA and (**B**) AA forcing only simulations shown in Fig. 4. The black (gray) stippling indicates that the correlation is statistically significant at the 0.05 (0.1) level based on a two-sided Student's t-test with an estimated effective degree of freedom to account for autocorrelation. Results are similar if the local, instead of PC1, SSTs from the model simulations were used.

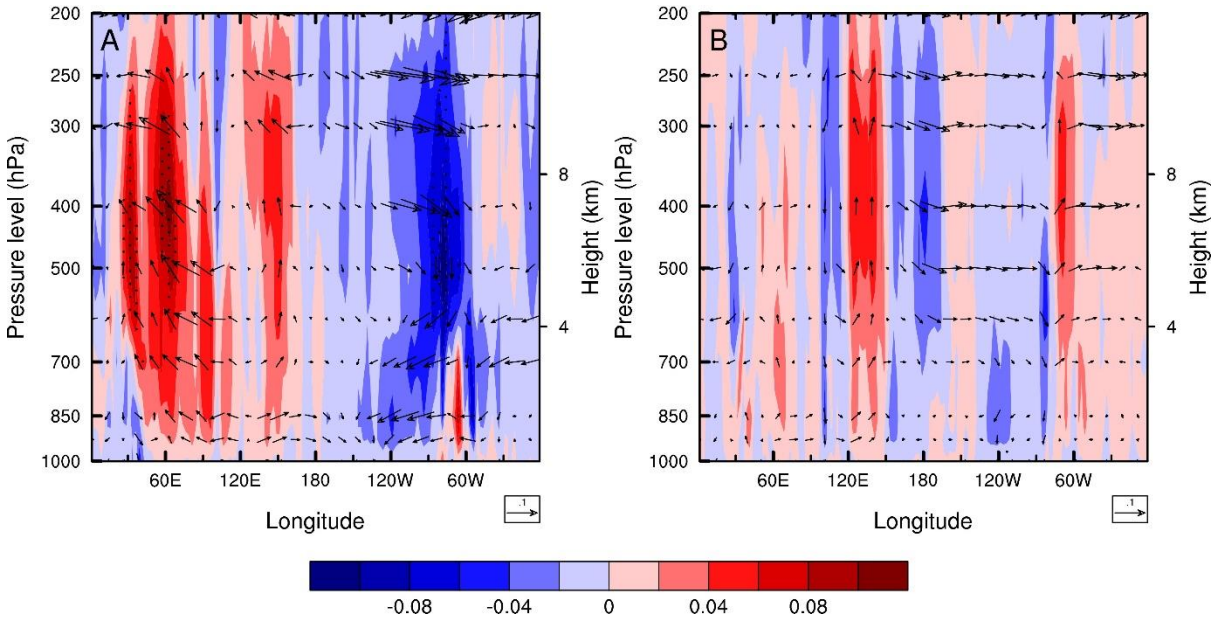

Fig. S4. Composite analysis of the atmospheric circulation. Height-longitude cross section of the annual-mean anomalies for the cold period (1965-1995) relative to the warm period (1935-1960) for (u, ω) wind changes averaged over 10°S–10°N from the MMM of the (**A**) CMIP5 and (**B**) CMIP6 simulations under AA forcing only (including models with aerosol indirect effects only). The model simulations were linearly detrended before calculating the anomalies. The stippling indicates that the anomalies are statistically significant at the 5% level based on a Student's t-test.

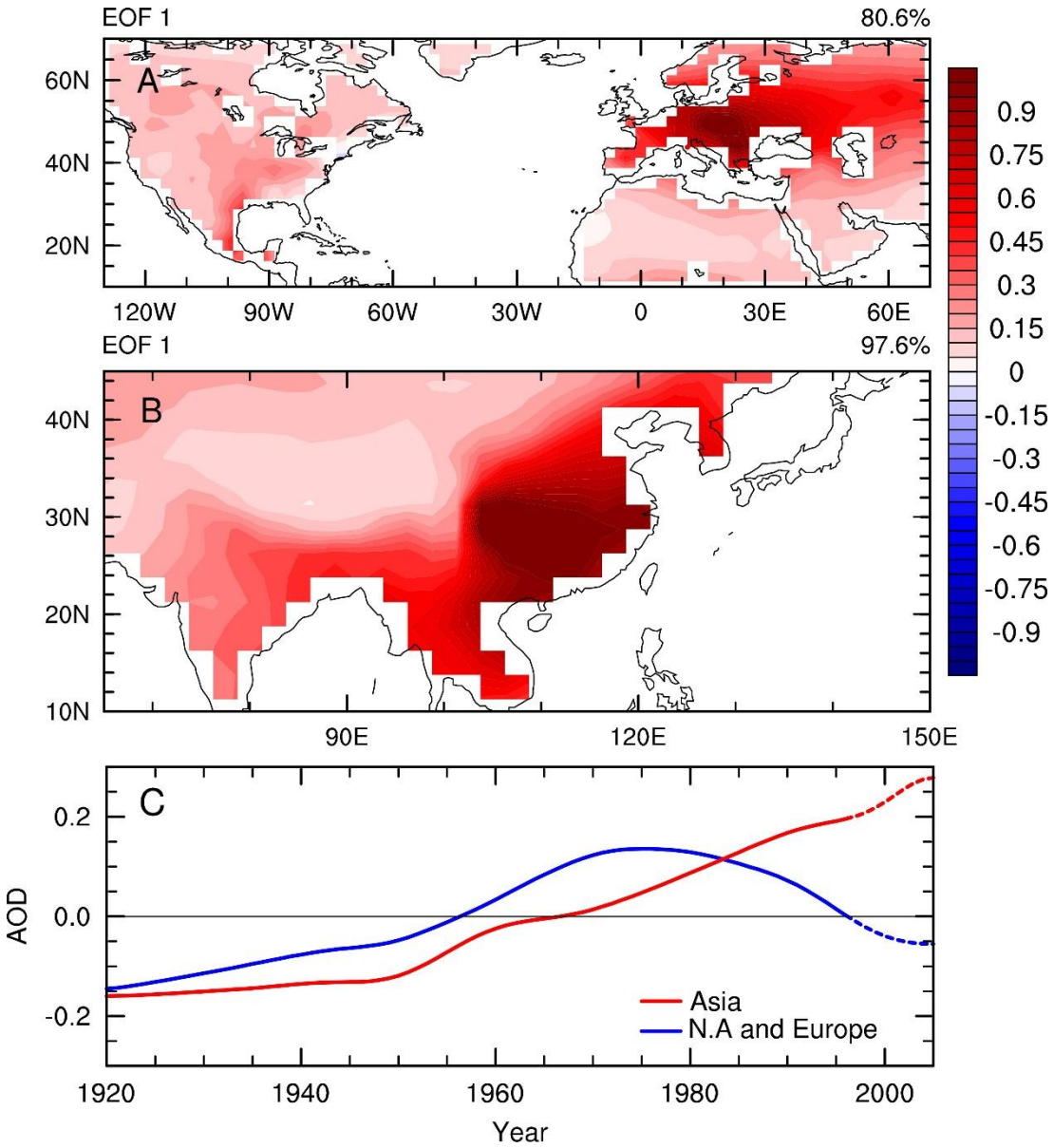

Fig. S5. Anthropogenic aerosol loading. Time series of the spatial pattern (**A**, **B**) and principal component (PC, **C**) of the leading EOF mode in the low-pass filtered ambient aerosol optical depth (AOD) at λ = 550 nm over (A) North America and Europe, and (B) East Asia using the data from the MMM of CMIP5 AA-forcing-only simulations from 1920-2005.

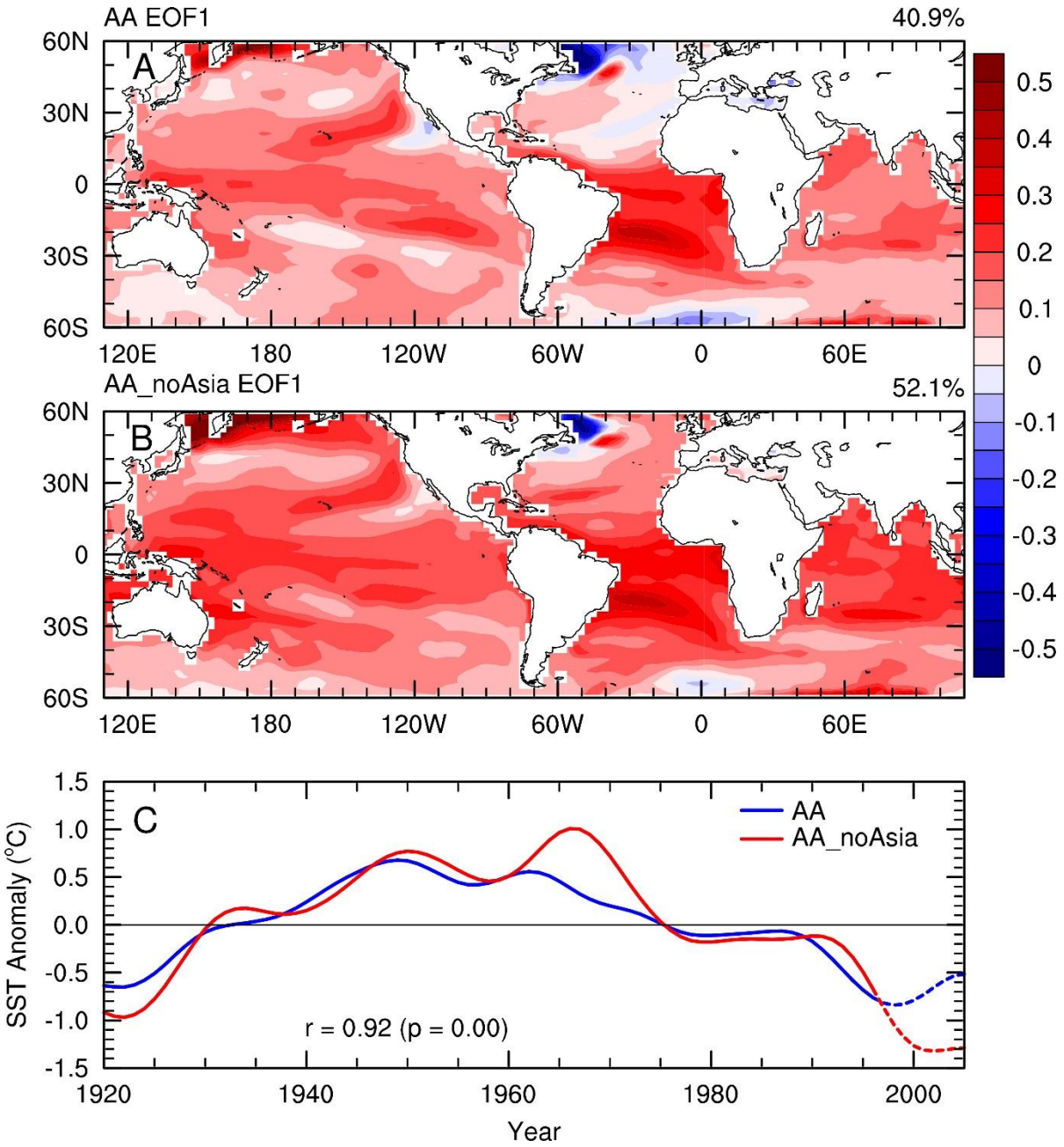

Fig. S6. Analysis of SST patterns with and without East Asian aerosols. Spatial patterns and time series of the principal component (PC) of the leading EOF mode in the near-global (60°S–60°N) linearly detrended, low-pass filtered SST fields from the CSIRO-Mk3.6.0 model simulations from 1920-2005 for (**A**) AA forcing only over the globe and (**B**) AA forcing only over the globe except East Asia (10°S–45°N, 65°E–150°E). The CSIRO-Mk3.6.0 model has parallel simulations in which anthropogenic aerosol emissions were prescribed either over the globe or over East Asia only. Here we used the difference between the two simulations to represent the response to aerosol emissions from outside East Asia in (B). The SST pattern remains broadly similar with and without East Asian aerosols. The data near the right end were derived with mirrored data in the filtering and thus are less reliable, they are marked by the dashed lines.

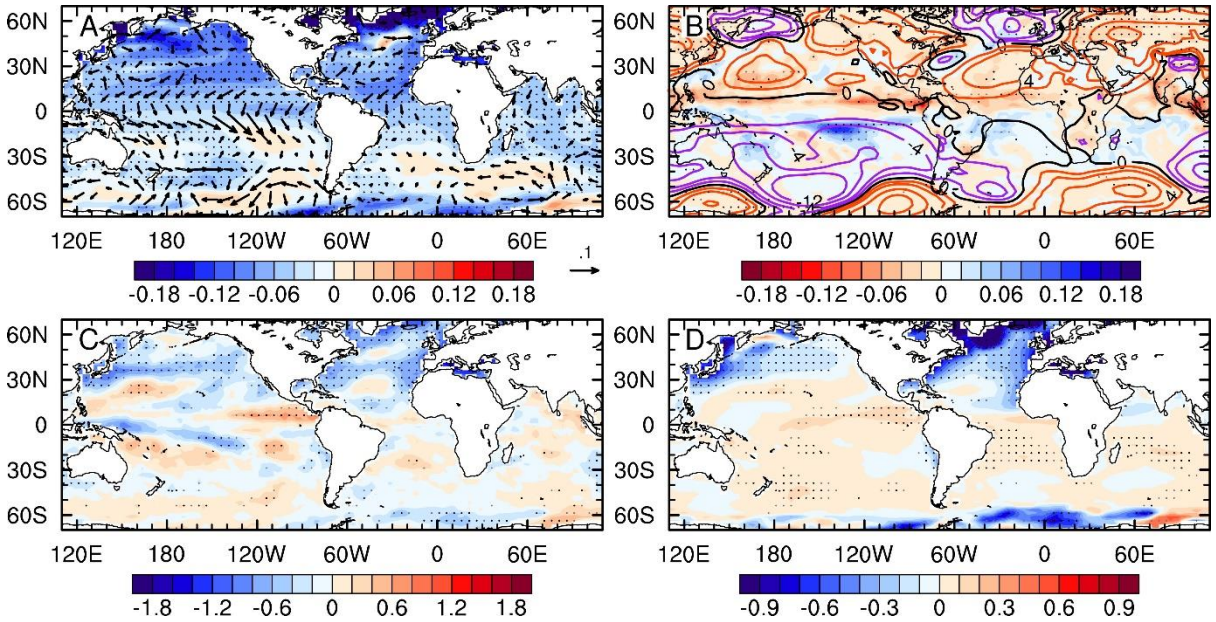

Fig. S7. Composite maps for SST, SLP and surface solar radiation. Annual-mean anomalies for the cold period (1965-1995) relative to the warm period (1935-1960) for (**A**) surface winds (vectors, m s^{-1}) and SST (°C, shading), (**B**) rainfall (mm day^{-1}, shading) and sea level pressure (SLP, hPa; black line represents the zero line, while purple and red lines represent the negative and positive contours, respectively), (**C**) surface net downward solar radiation (W m^{-2}), and (**D**) net clear-sky surface solar radiation (W m^{-2}) from the MMM of the CMIP6 AA-forcing-only simulations. The model simulations were linearly detrended before calculating the anomalies. The black (gray) stippling indicates that the correlation is statistically significant at the 0.05 (0.1) level based on a Student's t-test.

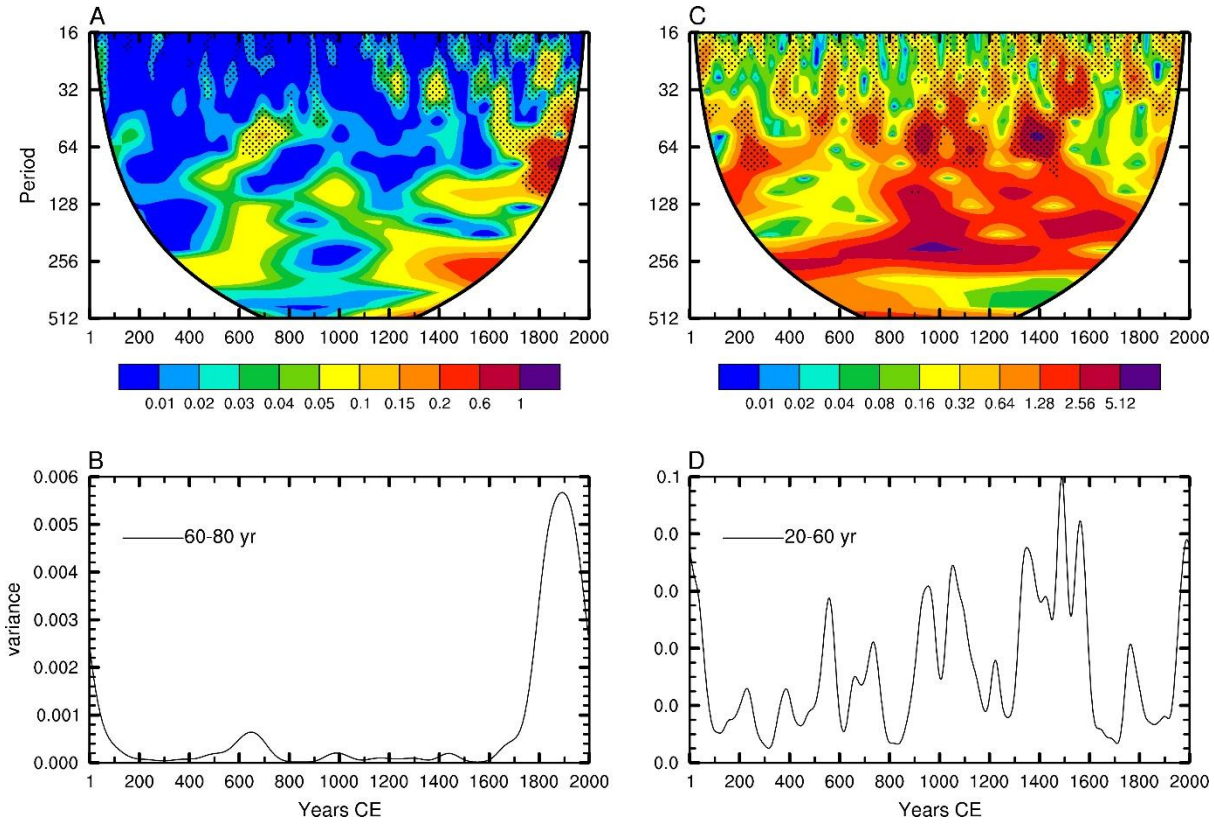

Fig. S8. Power spectra comparisons. (**A**) The wavelet power spectrum of the AMO index over the past two thousand years from the Paleo Hydrodynamics Data Assimilation product (PHYDA, *31*). The linear trend since year 1850 were removed before the analysis. We used a 19-point Lanczos filter with a 13-year cutoff period to smooth the AMO index data. (**B**) Scale-averaged wavelet power over the 60-80-year band for the AMO. (**C**, **D**): Same as (A, B), but for the Niño3.4 index and the 20-60-year power for the IPO. The black dots in (A) and (C) denote the 95% confidence level against a red noise.

Table S1. Summary of CMIP5 models used in this study. List of the 38 CMIP5 models with all-forcing historical and RCP4.5 future simulations. The number of ensemble simulations forced with individual historical forcing agents. We only used models with AA forcing that include aerosol indirect effects (AIE) associated with aerosol-cloud interactions.

No.	Model Name	forcing combinations					
		All	GHG	NAT	VA	SI	AA
1	ACCESS1.0	1					
2	ACCESS1.3	1					
3	bcc-csm1.1	1	1				
4	bcc-csm1.1-m	1					
5	BNU-ESM	1					
6	CanESM2	5	5	5		5	5
7	CCSM4	6		4	3	3	
8	CESM1-BGC	1					
9	CESM1-CAM5	3		3	3	2	3
10	CMCC-CM	1					
11	CMCC-CMS	1					
12	CNRM-CM5	1	6	6			
13	CSIRO-Mk3.6.0	10	5	5	5		5
14	FIO-ESM	3					
15	GFDL-CM2p1	10					
16	GFDL-CM3	1		3			3
17	GFDL-ESM2G	1					
18	GFDL-ESM2M	1					
19	GISS-E2-H-CC	1					
20	GISS-E2-H	16	5	5	10	10	
21	GISS-E2-R-CC	1					
22	GISS-E2-R	17	5	5	10	10	
23	HadCM3	10					
24	HadGEM2-CC	1					
25	HadGEM2-ES	4	4	4			
26	HadGEM2-AO	1					
27	inmcm4	1					
28	IPSL-CM5A-LR	4	3	3			
29	IPSL-CM5A-MR	1		3			
30	IPSL-CM5B-LR	1					
31	MIROC5	3					
32	MIROC-ESM-CHEM	1					
33	MIROC-ESM	1		3			
34	MPI-ESM-LR	3					
35	MPI-ESM-MR	3					
36	MRI-CGCM3	1					
37	NorESM1-ME	1					
38	NorESM1-M	1	1				

Table S2. Summary of CMIP6 models used in this study. The number of ensemble simulations by CMIP6 climate models forced with the anthropogenic aerosols (AA) and volcanic aerosols (VA).

Model Name	Ensemble runs AA/VA	Aerosol indirect effect
BCC-CSM2-MR	3	including the aerosol indirect effects in which the liquid cloud droplet number concentration is diagnosed using the aerosols masses; Radiative transfer scheme includes the aerosol indirect effects
CNRM-CM6-1	10	including the first indirect effect, prescribed
CanESM5	10/10	yes, including 1st and 2nd indirect effects
GISS-E2-1-G	5/5	the aerosol indirect effect is parameterized
HadGEM3-GC31-LL	4	yes, including 1st and 2nd indirect effects
IPSL-CM6A-LR	10	no indirect aerosol effect
MIROC6	3	yes, including 1st and 2nd indirect effects
MRI-ESM2-0	3	yes, including 1st and 2nd indirect effects
NorESM2-LM	3	yes, including 1st and 2nd indirect effects

REFERENCES AND NOTES

1. C. Deser, M. A. Alexander, S.-P. Xie, A. S. Phillips, Sea surface temperature variability: Patterns and mechanisms. *Ann. Rev. Mar. Sci.* **2**, 115–143 (2010).

2. D. Parker, C. Folland, A. Scaife, J. Knight, A. Colman, P. Baines, B. Dong, Decadal to multidecadal variability and the climate change background. *J. Geophys. Res.* **112**, D18115 (2007).

3. Z. Liu, Dynamics of interdecadal climate variability: A historical perspective. *J. Climate* **25**, 1963–1995 (2012).

4. W. Han, J. Vialard, M. J. McPhaden, T. Lee, Y. Masumoto, M. Feng, W. P. M. de Ruijter, Indian Ocean decadal variability: A review. *Bull. Am. Meteorol. Soc.* **95**, 1679–1703 (2014).

5. R. T. Sutton, G. D. McCarthy, J. Robson, B. Sinha, A. T. Archibald, L. J. Gray, Atlantic multidecadal variability and the U.K. ACSIS program. *Bull. Am. Meteorol. Soc.* **99**, 415–425 (2018).

6. R. Zhang, T. L. Delworth, Impact of Atlantic multidecadal oscillations on India/Sahel rainfall and Atlantic hurricanes. *Geophys. Res. Lett.* **33**, L17712 (2006).

7. B. Dong, A. Dai, The influence of the Interdecadal Pacific oscillation on temperature and precipitation over the globe. *Clim. Dynam.* **45**, 2667–2681 (2015).

8. C. Sun, F. Kucharski, J. Li, Western tropical Pacific multidecadal variability forced by the Atlantic Multidecadal Oscillation. *Nat. Commun.* **8**, 15998 (2017).

9. O. H. Otterå, M. Bentsen, H. Drange, L. Suo, External forcing as a metronome for Atlantic multidecadal variability. *Nat. Geosci.* **3**, 688–694 (2010).

10. B. B. B. Booth, N. J. Dunstone, P. R. Halloran, T. Andrews, N. Bellouin, Aerosols implicated as a prime driver of twentieth-century North Atlantic climate variability. *Nature* **484**, 228–232 (2012).

11. W. Hua, A. Dai, L. Zhou, M. Qin, H. Chen, An externally-forced decadal rainfall seesaw pattern over the Sahel and southeast Amazon. *Geophys. Res. Lett.* **46**, 923–932 (2019).

12. A. Bellucci, A. Mariotti, S. Gualdi, The role of forcings in the twentieth-century North Atlantic multidecadal variability: The 1940–75 North Atlantic cooling case study. *J. Climate* **30**, 7317–7337 (2017).

13. M. Watanabe, H. Tatebe, Reconciling roles of sulphate aerosol forcing and internal variability in Atlantic multidecadal climate changes. *Clim. Dynam.* **55**, 4651–4665 (2019).

14. X. Yan, R. Zhang, T. R. Knutson, A multivariate AMV index and associated discrepancies between observed and CMIP5 externally forced AMV. *Geophys. Res. Lett.* **46**, 4421–4431 (2019).

15. D. M. Smith, B. B. B. Booth, N. J. Dunstone, R. Eade, L. Hermanson, G. S. Jones, A. A. Scaife, K. L. Sheen, V. Thompson, Role of volcanic and anthropogenic aerosols in the recent global surface warming slowdown. *Nat. Clim. Chang.* **6**, 936–940 (2016).

16. J. Deng, A. Dai, H. Xu, Nonlinear climate responses to increasing CO_2 and anthropogenic aerosols simulated by CESM1. *J. Climate* **33**, 281–301 (2020).

17. W. Hua, A. Dai, M. Qin, Contributions of internal variability and external forcing to the recent Pacific decadal variations. *Geophys. Res. Lett.* **45**, 7084–7092 (2018).

18. D. B. Enfield, A. M. Mestas-Nuñez, P. J. Trimble, The Atlantic Multidecadal Oscillation and its relation to rainfall and river flows in the continental U.S. *Geophys. Res. Lett.* **28**, 2077–2080 (2001).

19. K. E. Trenberth, D. J. Shea, Atlantic hurricanes and natural variability in 2005. *Geophys. Res. Lett.* **33**, L12704 (2006).

20. T. L. Delworth, M. E. Mann, Observed and simulated multidecadal variability in the Northern Hemisphere. *Clim. Dynam.* **16**, 661–676 (2000).

21. J. R. Knight, R. J. Allan, C. K. Folland, M. Vellinga, M. E. Mann, A signature of persistent natural thermohaline circulation cycles in observed climate. *Geophys. Res. Lett.* **32**, L20708 (2005).

22. B. D. Santer, C. Bonfils, J. F. Painter, M. D. Zelinka, C. Mears, S. Solomon, G. A. Schmidt, J. C. Fyfe, J. N. S. Cole, L. Nazarenko, K. E. Taylor, F. J. Wentz, Volcanic contribution to decadal changes in tropospheric temperature. *Nat. Geosci.* **7**, 185–189 (2014).

23. N. Maher, S. McGregor, M. H. England, A. S. Gupta, Effects of volcanism on tropical variability, *Geophys. Res. Lett.* **42**, 6024–6033 (2015).

24. R. Zhang, T. L. Delworth, R. Sutton, D. L. R. Hodson, K. W. Dixon, I. M. Held, Y. Kushnir, J. Marshall, Y. Ming, R. Msadek, J. Robson, A. J. Rosati, M. Ting, G. A. Vecchi, Have aerosols caused the observed Atlantic Multidecadal Variability? *J. Atmos. Sci.* **70**, 1135–1144 (2013).

25. Y. Sato, D. Goto, T. Michibata, K. Suzuki, T. Takemura, H. Tomita, T. Nakajima, Aerosol effects on cloud water amounts were successfully simulated by a global cloud-system resolving model. *Nat. Commun.* **9**, 985 (2018).

26. S.-P. Xie, B. Lu, B. Xiang, Similar spatial patterns of climate responses to aerosol and greenhouse gas changes. *Nat. Geosci.* **6**, 828–832 (2013).

27. H. Wang, S.-P. Xie, Q. Liu, Comparison of climate response to anthropogenic aerosol versus greenhouse gas forcing: Distinct patterns. *J. Climate* **29**, 5175–5188 (2016).

28. S. McGregor, A. Timmermann, M. F. Stuecker, M. H. England, M. Merrifield, F.-F. Jin, Y. Chikamoto, Recent Walker circulation strengthening and Pacific cooling amplified by Atlantic warming. *Nat. Clim. Chang.* **4**, 888–892 (2014).

29. X. Li, S.-P. Xie, S. T. Gille, C. Yoo, Atlantic-induced pan-tropical climate change over the past three decades. *Nat. Clim. Chang.* **6**, 275–279 (2016).

30. G. W. K. Moore, J. Halfar, H. Majeed, W. Adey, A. Kronz, Amplification of the Atlantic Multidecadal Oscillation associated with the onset of the industrial-era warming. *Sci. Rep.* **7**, 40861 (2017).

31. N. J. Steiger, J. E. Smerdon, E. R. Cook, B. I. Cook, A reconstruction of global hydroclimate and dynamical variables over the Common Era. *Sci. Data* **5,** 180086 (2018).

32. R. Zhang, T. L. Delworth, Impact of the Atlantic multidecadal Oscillation on North Pacific climate variability. *Geophys. Res. Lett.* **34**, L23708 (2007).

33. C. K. Folland, D. E. Parker, F. E. Kates, Worldwide marine temperature fluctuations 1856–1981. *Nature* **310**, 670–673 (1984).

34. M. E. Schlesinger, N. Ramankutty, An oscillation in the global climate system of period 65–70 years. *Nature* **367**, 723–726 (1994).

35. R. A. Kerr, A North Atlantic climate pacemaker for the centuries. *Science* **288**, 1984–1985 (2000).

36. B. A. Steinman, M. E. Mann, S. K. Miller, Atlantic and Pacific multidecadal oscillations and Northern Hemisphere temperatures. *Science* **347**, 988–991 (2015).

37. B. B. Booth, Why the Pacific is cool. *Science* **347**, 952 (2015).

38. B. Huang, P. W. Thorne, V. F. Banzon, T. Boyer, G. Chepurin, J. H. Lawrimore, M. J. Menne, T. M. Smith, R. S. Vose, H.-M. Zhang, Extended Reconstructed Sea Surface Temperature version 5 (ERSSTv5), upgrades, validations, and intercomparisons. *J. Climate* **30**, 8179–8205 (2017).

39. N. A. Rayner, D. E. Parker, E. B. Horton, C. K. Folland, L. V. Alexander, D. P. Rowell, E. C. Kent, A. Kaplan, Global analyses of sea surface temperature, sea ice, and night marine air temperature since the late nineteenth century. *J. Geophys. Res. Atmos.* **108**, 4407 (2003).

40. A. Kaplan, M. A. Cane, Y. Kushnir, A. C. Clement, M. B. Blumenthal, B. Rajagopalan, Analyses of global sea surface temperature 1856-1991. *J. Geophys. Res.* **103**, 18567–18589 (1998).

41. S. Hirahara, M. Ishii, Y. Fukuda, Centennial-scale sea surface temperature analysis and its uncertainty. *J. Climate* **27**, 57–75 (2014).

42. K. E. Taylor, R. J. Stouffer, G. A. Meehl, An overview of CMIP5 and the experiment design. *Bull. Am. Meteorol. Soc.* **93**, 485–498 (2012).

43. J. E. Kay, C. Deser, A. Phillips, A. Mai, C. Hannay, G. Strand, J. M. Arblaster, S. C. Bates, G. Danabasoglu, J. Edwards, M. Holland, P. Kushner, J.-F. Lamarque, D. Lawrence, K. Lindsay, A. Middleton, E. Munoz, R. Neale, K. Oleson, L. Polvani, M. Vertenstein, The Community Earth System Model (CESM) Large Ensemble Project: A community resource for studying climate change in the presence of internal climate variability. *Bull. Am. Meteorol. Soc.* **96**, 1333–1349 (2015).

44. A. Dai, J. C. Fyfe, S.-P. Xie, X. Dai, Decadal modulation of global surface temperature by internal climate variability. *Nat. Clim. Chang.* **5**, 555–559 (2015).

45. A. Dai, C. E. Bloecker, Impacts of internal variability on temperature and precipitation trends in large ensemble simulations by two climate models. *Clim. Dynam.* **52**, 289–306 (2019).

46. B. J. Pyper, R. M. Peterman, Comparison of methods to account for autocorrelation in correlation analyses of fish data. *Can. J. Fish. Aquat. Sci.* **55**, 2127–2140 (1998).

47. W. Zhao, M. A. K. Khalil, The relationship between precipitation and temperature over the contiguous United States. *J. Climate* **6**, 1232–1236 (1993).

48. L. Dong, T. Zhou, B. Wu, Indian Ocean warming during 1958–2004 simulated by a climate system model and its mechanism. *Clim. Dynam.* **42**, 203–217 (2014).